Quantitative Real-Space Analysis of Self-Assembled Structures of Magnetic Dipolar Colloids

Mark Klokkenburg, Roel P. A. Dullens, Willem K. Kegel, Ben H. Erné, and Albert P. Philipse
Van 't Hoff Laboratory for Physical and Colloid Chemistry, Debye Institute, Utrecht University, Padualaan 8, 3584 CH Utrecht, The Netherlands
(Received 12 August 2005; published 24 January 2006)

We present the first real-space analysis on a single-particle level of the dipolar chains and branched clusters self-assembling in magnetic fluids in zero field. Spatial correlations and chain-length distributions directly obtained from tracked particle positions in vitrified films of synthetic magnetic (Fe_3O_4) dispersions provide a quantitative test for simulations and theory of dipolar fluids. A pertinent example is the cluster-size distribution that can be analyzed with a one-dimensional aggregation model to yield a dipolar attraction energy that agrees well with the dipole moment found from independent magnetization measurements.

DOI: 10.1103/PhysRevLett.96.037203 PACS numbers: 75.50.Mm, 64.70.Nd, 82.70.Dd

The equilibrium statistical thermodynamics of dipolar colloidal fluids still contains controversial topics despite a long history of theory and simulations [1]. The prediction of liquid-gas criticality for spheres with a permanent magnetic moment [2], for example, has not been validated by simulations. Most of them [3–6] (but not all [7]) fail to find liquid-gas coexistence driven by isotropic aggregation. Instead, they reveal self-assembly of particles into dipolar chains that do not seem to macroscopically phase separate. Several theories [1,8–10] support this chain-formation scenario, though an alternative phase coexistence between a gas of chain ends and a high-density liquid of chain branching points was proposed [11].

Quite striking in the long-standing study of permanent colloidal dipoles is the complete absence of quantitative real-space information from experiments on dipolar structures for real magnetic colloids. The main reason is that the dipolar particles *in computero,* namely monodisperse hard spheres with a tunable, permanent magnetic moment, are difficult to realize in the laboratory. Only recently the predicted dipolar chains in zero field [2] have been imaged *in situ* for superparamagnetic iron colloids [12,13]. However, quantifying dipolar structures on the desired single-particle level is for the iron particles obstructed by the irregular particle shape and their extreme sensitivity to oxidation.

Here, we report a quantitative study of dipolar structures from recently developed, well-defined, single-domain magnetite (Fe_3O_4) colloids with adjustable size and, consequently, tunable permanent magnetic dipole moment that spontaneously self-assemble into a variety of dipolar structures [14]. Our primary goal is to show that this type of magnetic fluid yields the equilibrium distributions of particle positions that can be directly—and quantitatively—compared to theory and simulations. As an illustration, we analyze experimental chain-length distributions with a one-dimensional aggregation model, exact in the limit of reversible, straight chains containing nearest-neighbor attractions only.

Images of dipolar structures can be obtained by cryogenic transmission electron microscopy (cryo-TEM) [12,14] of thin (2D) vitrified films of colloidal dispersions of magnetic nanoparticles, so-called ferrofluids [15]. Steric stabilization of these particles in nonpolar solvents substantially screens van der Waals attractions and introduces steep steric repulsion between the particles at contact. Therefore, the additional contribution to the pair interaction is a dipolar potential x/r^3, where x is the amplitude depending on the angular orientation of two dipoles at a center-to-center distance r [15]. The maximal dipolar attraction (for two dipoles in head-to-tail configuration) is $V_{\max} = -\mu_0\mu^2/2\pi k_B T\sigma^3$, where $\mu_0 = 4\pi \times 10^{-7}\ \mathrm{J\,A^{-2}\,m^{-1}}$, μ is the magnetic dipole moment of one particle, k_B is the Boltzmann constant, T is the absolute temperature, and σ is the hard core diameter.

Three colloidal magnetite dispersions (A, B, and C) in Decalin were prepared by a method described previously [14]. The average particle diameter (d) according to TEM (including the 2 nm thick surfactant layer) and the particle concentration expressed in surface fraction θ ($= N_T A_p/A_I$, where N_T is the total number of particles in the images, A_p is the cross-sectional area of one particle, and A_I is the total area of all images) are listed in Table I. In addition, the values for the dipolar contact attraction $V_{\max}$ are given using the measured dipole moment of the particles, $4.8 \times 10^5\ \mathrm{A\,m^{-1}}$ for the magnetization saturation per unit volume for magnetite, and the interparticle distance obtained

TABLE I. The average particle size d and pair interaction energy $V_{\max}$ of systems A and B.

Code	Particle diameter d (nm)	Pair interaction energy $V_{\max}$ (k_BT)	Surface energy θ
A	20 ± 2.6	-4	0.14
B	24 ± 2.4	-9	0.14
C	24 ± 2.4	-9	0.03

from radial distribution [$g(r)$] data (see Fig. 2 below). Cryo-TEM images (Fig. 1) were obtained for system A, B, and a 4.5 times diluted dispersion of B, which is referred to as C. Note that the average breakup time of the dipolar structures (on the order of 0.02 s) is much smaller than the preparation time of several seconds of the cryo-TEM film (2D) before it is vitrified [12,14]. To track particle positions in 2D snapshots, we used image analysis software [16]. For system A, 6 images were analyzed containing altogether 1973 particles, for system B, 3723 particle centers were collected from 9 images, and for system C, 1357 particles were tracked from 10 images.

The cryo-TEM images (Fig. 1) of systems A and B clearly demonstrate the effect of increasing dipolar attractions. In system A, where on average $V_{\max} = -4$ (Table I) and, consequently, the dipolar attraction does not fully dominate, a substantial number of particles forms clusters with an irregular conformation. These clusters may be considered as the onset of dipolar chain formation. In contrast, in system B ($V_{\max} = -9$) the dipolar attractions dominate and anisotropic features appear due to the favorable head-to-tail orientations. The structures that form are flexible chains, branched chains, and flux-closure rings, i.e., the type of structures also seen in 2D [3,17,18] and 3D [4,6] simulations. Despite the high number of branching points, usually referred to as defects [11], most particles are still linearly connected. System C [Fig. 1(c)] shows that the dipolar chains partially dissociate when the system is diluted, which demonstrates that Fig. 1 displays thermodynamic equilibrium structures.

As a first quantification of the observed structures, we calculated the radial distribution function $g(r)$ from the cryo-TEM images, which is presented in Fig. 2. The data show for the smallest A particles only one peak at a distance $r/d = 1$, manifesting small structures only. Based on $W(r) = -k_B T \ln[g(r)]$, where $W(r)$ is the potential of mean force, the interactions between the particles are of the order of $k_B T$, which corroborates measured dipole moments of the A particles (Table I). The stronger dipolar attractions for the larger B particles lead to more pronounced peaks in $g(r)$ due to linear trimers or repeating dimers in large networks. Note that $g(r)$ maxima are located close to integer values of the particle diameter, indicating the predominance of linear aggregation. Furthermore, the first peak in B is rather sharp and well defined, which is the result of the relatively strong particle attraction energy ($V_{\max} = -9$). Upon dilution (C), the correlations at short distances become more pronounced at the cost of correlations at longer distances. Our results qualitatively confirm those predicted by simulations on dipolar fluids [18,19].

To better highlight the effect of particle size and concentration on the topology, we calculated the number of nearest neighbors per particle (Fig. 3), defining a neighbor as being located within a center-to-center distance of $r_c = 1.35d$. The calculations were not affected by the choice of the cutoff distance in the range $1.0d$–$1.5d$. For system B, the distribution (Fig. 3) sharply peaks at $N_c = 2$, indicating the one-dimensional character of the structures. The increased linearity is corroborated by the average coordination number of system B which is 2.17, compared to 2.62 found for ferrofluid A. The average coordination number for C is 0.95, signaling the dissociation of dipolar chains into shorter ones, resulting in more single particles, and fewer clusters with defects. Indeed, Fig. 3 shows that the probability of having zero neighbors in C is much higher than in A or B and, furthermore, there no longer is a maximum at $N_c = 2$.

To examine the size and shape of the individual self-assembled structures, we first make a distinction between chains and clusters. A chain is an entity that has at least one *end particle* that has only one nearest neighbor. The other

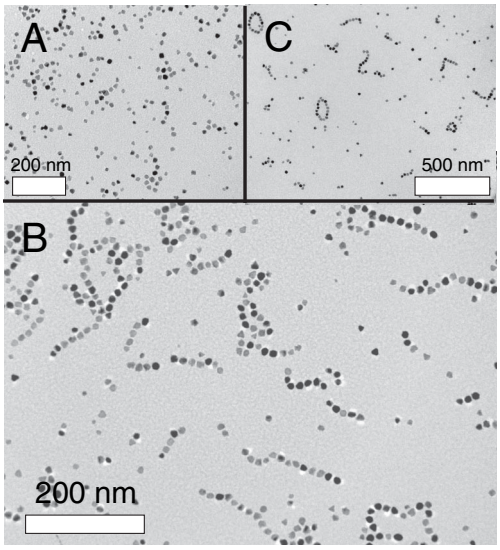

FIG. 1. Typical *in situ* cryo-TEM images of vitrified magnetite dispersions A, B, and C. The surface fraction is 0.14 for systems A and B, and 0.03 for system C.

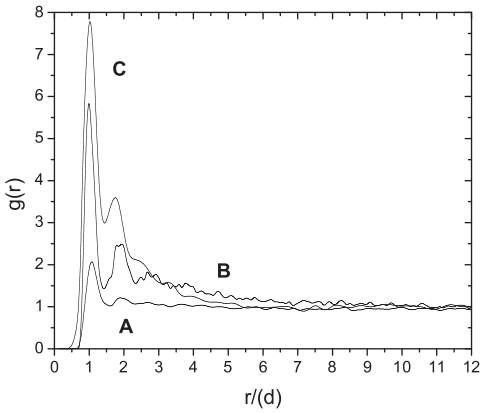

FIG. 2. Radial distribution functions $g(r)$ obtained from the cryogenic 2D snapshots for different attractions V and different surface fractions θ (see Table I).

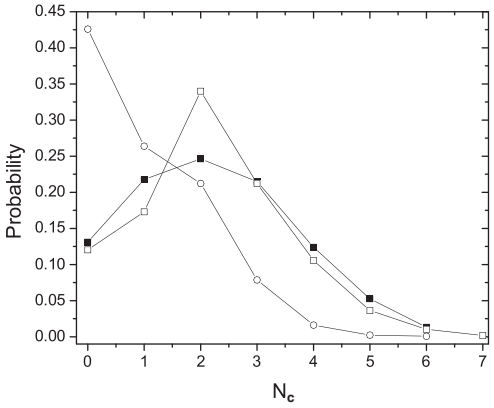

FIG. 3. Histograms of the coordination number N_c probability of a particle in ferrofluid A (■), B (□), and C (○). Note that the coordination number probability of B sharply peaks at $N_c = 2$, indicating the presence of linear structures.

end of the chain is either another end particle or a *defect particle,* defined as a particle that has more than two neighbors. The ends of a chain are connected by *interior particles* that have only two nearest neighbors. A cluster has one end particle that serves as a starting point; all the nearest neighbors of this particle are assigned to be part of this cluster, including their nearest neighbors, etc., until no new neighbors are detected. These definitions imply that a chain can be a part of a cluster.

First, the deflections of the as-defined magnetic chains are quantified by the ratio α of the shortest end-to-end distance, to the total contour length $(n-1)d$ of an n-particle chain. Values for α [Fig. 4(a)] demonstrate the considerable and comparable chain curvature for A and B. Similar data were obtained for system C. The mean values of α for the chains in systems A, B, and C are 0.92, 0.93, and 0.93, respectively. Second, to elucidate the cluster topology in systems A and B, we calculated the average coordination number per cluster as a function of the cluster size. The average coordination number [Fig. 4(b)] in a cluster increases as the cluster size grows. For system A the mean coordination number approaches 2.4 for long clusters, whereas for B and C (not shown) the limit is 2.1. These numbers indicate a more irregular shape of the structures in A. A comparison with coordination numbers for two limiting cases, namely, a rigid chain (1D) and a hexagonal cluster (2D) [Fig. 4(b)], further confirms that the structures in A and B have a pronounced one-dimensional character due to the dominating dipolar interparticle attraction.

In addition, we determined the chain and cluster-size distributions, as shown in Fig. 5. The obtained chain-length distributions for the three systems all exponentially decay with an increasing number of particles in a chain [see inset of Fig. 5(a)]. The average chain length for system A is 3.6 particles, whereas for system B it is 4.2 particles. The chain-length probability in ferrofluid C decays faster with

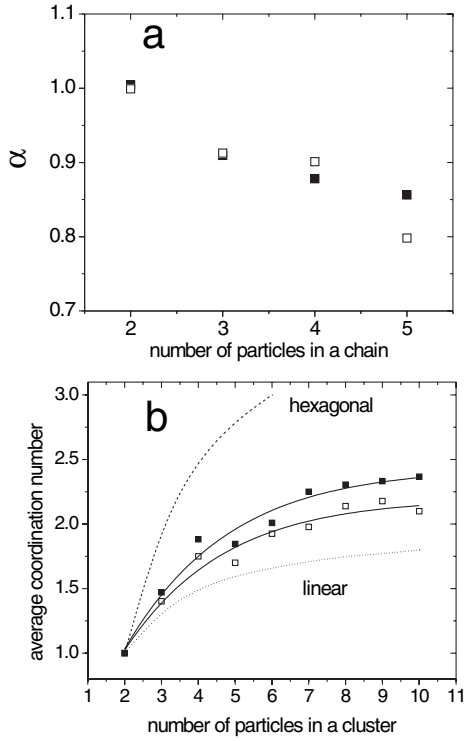

FIG. 4. (a) The deflection of the chains in terms of the ratio α, of the end-to-end distance to the total contour length $(n-1)d$, versus the number of particles n in a chain for systems A (■) and B (□). (b) Average coordination number per cluster as a function of cluster size for systems A (■) and B (□). Two limiting cases for the average coordination number in one and two dimensions are included: linear chains (dotted line) and hexagonal clusters (dashed line). The lines through the data points are a guide to the eye.

increasing length and indicates the presence of significantly more single particles compared to A and B. Consistently, the average length is reduced from 4.2 to 1.7 particles due to dilution by a factor of 4.5. The cluster-size distributions [Fig. 5(b)] are similar to the chain-length distributions. The average cluster sizes are 4.2 and 4.9 particles for systems A and B, respectively. Note that the chain-length and the cluster-size probabilities for system C are almost identical, which also follows from the average cluster size of 1.7 particles. Size distributions of structures obtained by simulations in 2D [17] and 3D [5], where the clarifying distinction between clusters and chains is not made, predict similar decays with increasing length at low density.

For an equilibrium distribution between colloids (monomers) and linear rigid chains, taking into account only the effective nearest-neighbor interaction energy V, the law of mass action yields the exact result

$$x_q = x_1^q \exp(-(q-1)V), \tag{1}$$

where x_1 is the surface mole fraction (the film thickness is close to 1 particle diameter) of single particles, and V is

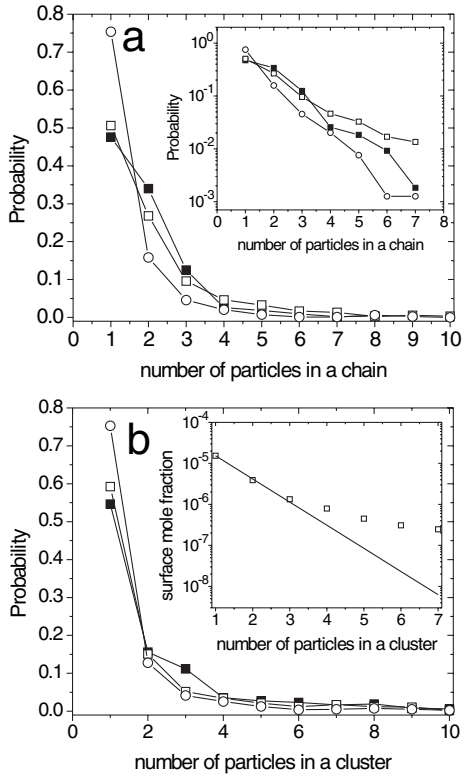

FIG. 5. (a) The chain-length distribution for systems A (■), B (□), and C (○). The inset shows the chain-length distribution on a logarithmic scale. (b) The cluster-size distributions for system A (■), B (□), and C (○). The inset shows a fit to the data obtained for system B according to Eq. (1).

dimensionless and scaled to thermal energy. This distribution (applied earlier to surfactants [20]) agrees with the initial exponential decay in our own data [inset in Fig. 5(b)], whereas it deviates for chains with $n \geq 4$. This deviation is obviously due to the flexibility and branching disregarded in Eq. (1). The fit to the initial decay, however, yields -9.8 for V, which quantitatively agrees with V calculated from the independently measured dipole moment of the particles (Table I). As consistency requires, the data obtained for system C (fit not shown) yield a very similar value for the attraction V. By solving Eq. (1) for x_1, we verified that its value agrees with the experimentally obtained monomer concentration. Analysis of the data of system A resulted in unrealistic values for the pair interaction. This is expected since this system hardly forms one-dimensional chains. Note that the relevant thermodynamic measure for concentration in this model is surface mole fraction [21].

In conclusion, we have demonstrated a quantitative real-space analysis of magnetic equilibrium structures on a single-particle level that can be directly compared to theory and simulations on dipolar fluids. The presented magnetic colloidal system shows that strongly dipolar colloids self-assemble to flexible chains as well as branched clusters with a pronounced linear character. In the dilute regime, a transition occurs to predominantly unbranched structures. From the cluster-size distributions for strongly dipolar fluids, the pair interaction can be determined from a one-dimensional aggregation model. We find no evidence in the cryo-TEM images for liquid-gas coexistence driven by isotropic forces. Future work will address the much debated effect of polydispersity [22] on the magnetic equilibrium-size distributions.

We thank J. Meeldijk for his help with the cryo-TEM experiments and D. Aarts for fruitful discussions.

[1] P. I. C. Teixeira, J. M. Tavares, and M. M. Telo da Gama, J. Phys. Condens. Matter **12**, R411 (2000).
[2] P. G. de Gennes and P. Pincus, Phys. Kondens. Mater. **11**, 189 (1970).
[3] R. W. Chantrell, A. Bradbury, J. Popplewell, and S. W. Charles, J. Phys. D **13**, L119 (1980).
[4] J. J. Weis and D. Levesque, Phys. Rev. Lett. **71**, 2729 (1993).
[5] J. M. Tavares, J. J. Weis, and M. M. Telo da Gama, Phys. Rev. E **59**, 4388 (1999).
[6] Z. Wang, C. Holm, and H. W. Müller, Phys. Rev. E **66**, 021405 (2002).
[7] P. J. Camp, J. C. Shelley, and G. N. Patey, Phys. Rev. Lett. **84**, 115 (2000).
[8] R. van Roij, Phys. Rev. Lett. **76**, 3348 (1996).
[9] V. S. Mendelev and A. O. Ivanov, Phys. Rev. E **70**, 051502 (2004).
[10] A. O. Ivanov, Z. Wang, and C. Holm, Phys. Rev. E **69**, 031206 (2004).
[11] T. Tlusty and S. A. Safran, Science **290**, 1328 (2000).
[12] K. Butter, P. H. H. Bomans, P. M. Frederik, G. J. Vroege, and A. P. Philipse, Nat. Mater. **2**, 88 (2003).
[13] K. Butter, P. H. Bomans, P. M. Frederik, G. J. Vroege, and A. P. Philipse, J. Phys. Condens. Matter **15**, S1451 (2003).
[14] M. Klokkenburg, C. Vonk, E. M. Claesson, J. D. Meeldijk, B. H. Erné, and A. P. Philipse, J. Am. Chem. Soc. **126**, 16 706 (2004).
[15] R. E. Rosensweig, Sci. Am. **247**, No. 10, 124 (1982).
[16] J. C. Crocker and D. G. Grier, J. Colloid Interface Sci. **179**, 298 (1996).
[17] J. M. Tavares, J. J. Weis, and M. M. Telo da Gama, Phys. Rev. E **65**, 061201 (2002).
[18] P. D. Duncan and P. J. Camp, J. Chem. Phys. **121**, 11 322 (2004).
[19] M. J. Stevens and G. S. Grest, Phys. Rev. E **51**, 5962 (1995).
[20] J. Israelachvilli, *Intermolecular and Surface Forces* (Academic Press, San Diego, 1992), pp. 341–360.
[21] H. Reiss, W. K. Kegel, and J. Groenewold, Ber. Bunsen-Ges. Phys. Chem. **100**, 279 (1996).
[22] A. O. Ivanov and S. S. Kantorovich, Phys. Rev. E **70**, 021401 (2004).